Video Article

Fabrication of High Contrast Gratings for the Spectrum Splitting Dispersive Element in a Concentrated Photovoltaic System

Yuhan Yao[1], He Liu[1], Wei Wu[1]

[1]Department of Electrical Engineering, University of Sothern California

Correspondence to: Wei Wu at wu.w@usc.edu

URL: http://www.jove.com/video/52913
DOI: doi:10.3791/52913

Keywords: Parallel spectrum splitting, dispersive element, high contrast grating, concentrated photovoltaic system, nanoimprint lithography, reactive ion etching

Date Published: 4/23/2015

Citation: Yao, Y., Liu, H., Wu, W. Fabrication of High Contrast Gratings for the Spectrum Splitting Dispersive Element in a Concentrated Photovoltaic System. *J. Vis. Exp.* (), e52913, doi:10.3791/52913 (2015).

Abstract

High contrast gratings are designed and fabricated and its application is proposed in a parallel spectrum splitting dispersive element that can improve the solar conversion efficiency of a concentrated photovoltaic system. The proposed system will also lower the solar cell cost in the concentrated photovoltaic system by replacing the expensive tandem solar cells with the cost-effective single junction solar cells. The structures and the parameters of high contrast gratings for the dispersive elements were numerically optimized. The large-area fabrication of high contrast gratings was experimentally demonstrated using nanoimprint lithography and dry etching. The quality of grating material and the performance of the fabricated device were both experimentally characterized. By analyzing the measurement results, the possible side effects from the fabrication processes are discussed and several methods that have the potential to improve the fabrication processes are proposed, which can help to increase the optical efficiency of the fabricated devices.

Video Link

The video component of this article can be found at http://www.jove.com/video/52913/

Introduction

Our modern society will not survive without moving a significant portion of energy consumption to renewable energy sources. To make this happen, we have to find a way to harvest renewable energy at a cost lower than petroleum-based energy sources in the near future. Solar energy is the most abundant renewable energy on earth. Despite that a lot of progresses have been made in solar energy harvesting, it is still very challenging to compete with petroleum-based energy sources. Improving the efficiency of solar cells is one of the most efficient ways to lower the system cost of solar energy harvesting.

Optical lenses and dish reflectors are usually used in most concentrated photovoltaic (CPV) systems[1] to achieve a high concentration of solar power incidence on the small-area solar cells, so it is economically viable to exploit expensive tandem multi-junction solar cells[2] in CPV systems, and to maintain a reasonable cost at the same time. However, for most non-concentrated photovoltaic systems, which usually require a large-area installment of solar cells, the high-cost tandem solar cells cannot be incorporated, although they usually have a broader solar spectrum response and a higher overall conversion efficiency than the single junction solar cells[3].

Recently, with the help of the parallel spectrum splitting optics (*i.e.* dispersive element), the parallel spectrum splitting photovoltaic technology[4] has made it possible that a similar or better spectrum coverage and conversion efficiency can be achieved without using the expensive tandem solar cells. The solar spectrum can be split into different bands and each band can be absorbed and converted to electricity by the specialized single-junction solar cells. In this way, the expensive tandem solar cells in CPV systems can be replaced by a parallel distribution of single-junction solar cells without any compromise on the performance.

The dispersive element that was designed in this report can be applied in a reflective CPV system (which is based on dish reflectors) to realize parallel spectrum splitting for the improved solar-electricity conversion efficiency and reduced cost. Multilayer high contrast gratings (HCG)[5] is used as the dispersive element by designing each layer of HCG to work as an optical band reflector. The structures and parameters of the dispersive element are numerically optimized. Moreover, the fabrication of high contrast gratings for the dispersive element by using dielectric (TiO_2) sputtering, nanoimprint lithography[6] and reactive ion etching is studied and demonstrated.

Protocol

1. Prepare the Blank Polydimethylsiloxane (PDMS) Substrate for Nanoimprint Mold

1. Silicon wafer treatment process

1. Clean a 4-inch silicon wafer by rinsing with acetone, methanol and isopropanol.
2. Blow it dry using the nitrogen gun.
3. Clean it using piranha solution (3:1 mixture of sulfuric acid with 30% hydrogen peroxide) by soaking inside for 15 min.
4. Rinse it with DI water. Blow dry using the nitrogen gun.
5. Place the wafer in a glass desiccator. Add a drop (20 drops = 1 ml) of releasing agent (trichlorosilane) into the desiccator.
6. Pump down the desiccator until the gauge reads -762 Torr and wait for 5 hr.
7. Take the wafer out, which has been treated with releasing agent.

2. Preparation of PDMS film (used as mold in nanoimprint)
   1. Weigh 10 g of silicone elastomer base and 1 g of curing agent.
   2. Add them in the same glass beaker.
   3. Stir and mix with a glass rod for 5 min.
   4. Put the mixture into a vacuum desiccator until the gauge reads -762 Torr to pump out all the trapped air bubbles.
   5. Spread them evenly onto the treated 4-inch silicon wafer.
   6. Bake the wafer with PDMS on top in the vacuum oven for 7 hr at 80 °C to cure the PDMS film.

2. Prepare the Nanoimprint Mold (Duplication from the Master Mold)

1. Spin twelve drops (20 drops = 1 ml) of UV curable resist (15.2%) on a clean blank silicon wafer for 30 sec at 1,500 rpm.
2. Carefully peel a piece of PDMS film off the treated silicon wafer.
3. Put the PDMS film onto the UV curable resist and let it absorb the UV resist for 5 min then peel it off.
4. Repeat 2.1 - 2.3 on the same PDMS film for two times. Absorb the UV resist for 3 min and 1 min respectively.
5. Place the PDMS film (after three-time UV resist absorption) onto a silicon master mold.
6. Put it into a chamber with nitrogen environment.
7. Turn on UV lamp to cure the sample for 5 min.
8. Peel off the PDMS film. The cured UV resist on the PDMS will keep the negative pattern of the master mold.
9. Use RF O_2 plasma to treat the PDMS mold. (RF power: 30 W, pressure: 260 mTorr, time: 1 min)
10. Place the PDMS mold in a vacuum chamber with one drop (20 drops = 1 ml) of releasing agent for 2 hr.

3. Nanoimprint Pattern Transfer

1. Spin eight drops (20 drops = 1 ml) of PMMA (996k, 3.1%) on the substrate to be imprinted for 50 sec at 3,500 rpm.
2. Bake it on a hotplate for 5 min at 120 °C.
3. Wait for the sample to cool down.
4. Spin eight drops (20 drops = 1 ml) of UV curable resist (3.9%) on the same substrate.
5. Place the PDMS mold (prepared in step 2) onto the sample (with both UV resist and PMMA).
6. Put it into a chamber with nitrogen environment.
7. Turn on the UV lamp to cure for 5 min.
8. Peel the PDMS mold off the sample and the pattern on the PDMS mold gets transferred to the sample.

4. Cr Lift-off Process

1. Reactive ion etching residual layer of UV resist and PMMA
   Note: The SOP for ICP machine can be found at https://www.nanocenter.umd.edu/equipment/fablab/sops/etch-07/Oxford%20Chlorine%20Etcher%20SOP.pdf
   1. Log in RIE ICP machine.
   2. Load a blank 4-inch silicon wafer. Run the clean recipe for 10 min.
   3. Take the blank silicon wafer out.
   4. Mount the sample on another clean silicon wafer and load it into the machine.
   5. Run the UV resist etching recipe for 2 min (the recipe can be found in **Table 1**).
   6. Take the sample out. Load a blank 4-inch silicon wafer. Re-run the clean recipe (can be found in **Table 1**) for 10 min.
   7. Mount the sample on a clean silicon wafer and load it into the machine.
   8. Run the PMMA etching recipe (can be found in **Table 1**) for 2 min.
      Note: Now the residual resist has been etched and substrate is exposed.

2. Cr e-beam evaporation
   1. Log into e-beam evaporator.
   2. Load the Cr metal source and sample into the chamber.
   3. Set the thickness (20 nm) and deposition rate (0.03 nm/sec).
   4. Pump the chamber until required vacuum (10^{-7} Torr) is reached.
   5. Start the deposition process.
   6. Take the sample out after the deposition finishes.

3. Cr lift-off procedure
   1. Immerse the sample in acetone with ultrasonic agitation for 5 min.
   2. Clean the sample by rinsing with acetone, methanol and isopropanol.

Note: The Cr evaporated on the resist will be lifted off and a Cr mask for substrate etching is formed.

5. TiO_2 Deposition

1. Load sample.
2. Set the parameters for the direct current magnetron sputtering machine
    1. Use a chamber pressure of 1.5 mTorr, Ar flow of 100 sccm and a sputtering power of 130 W.
    2. Use a temperature of 27 °C and a stage rotation speed of 20 rpm.
3. Start the sputter process and stop at desired thickness.
4. Take the sample out and anneal the TiO_2 film in oxygen environment at 300 °C for 3 hr.

6. High Contrast Grating Etching

1. Log in the inductively coupled plasma (ICP) reactive ion etching (RIE) machine.
2. TiO_2 etching
    1. Load a blank 4-inch silicon wafer.
    2. Start and run the clean recipe (can be found in **Table 1**) for 10 min.
    3. Unload load the blank wafer and load the sample with Cr mask.
    4. Set etching time. Start TiO_2 etching recipe. The etching process will automatically stop.
    5. Unload the sample.
3. SiO_2 etching
    1. Repeat step 5.2 except use the SiO_2 etching recipe.

7. Reflectance Measurement

1. Log in and turn on the measurement system.
2. Place the reflectance standard mirror on the sample holder and align the optical path.
3. Calibrate the system for the 100% reflectance.
4. Take off the reflectance standard mirror and place the HCG.
5. Measure the reflectance of the HCG.
6. Save the data and log out of the measurement system.

Representative Results

Figure 1 shows the implementation of the dispersive element (multilayer high contrast grating (HCG)) in a concentrated photovoltaic system. The sun light is first reflected by the primary mirror and impinges on the reflective dispersive element, where the beam is reflected and split into different bands of different wavelengths. Each band will impinge on a certain location on the solar cell array for the best absorption and conversion to electricity. The key to this system is the design and implementation of the dispersive element, which is composed of multiple layers of HCG.

Figure 2 shows the numerical optimization result for each layer in the dispersive element. The results was calculated by the finite-difference time-domain (FDTD)[7] based commercial simulation software “Lumerical” and further validated by rigorous coupled-wave analysis (RCWA)[8]. The refractive index of TiO_2 was from the SOPRA[9] online database. The optimized six-layer dispersive element can provide a total reflection of more than 90% over the entire solar spectrum.[10,11]

To demonstrate the broadband reflectance of HCG experimentally, one of the six layers in the dispersive element HCG structure is fabricated using nanoimprint fabrication. As shown in **Figure 3**, each grating block consists of two parts. The material of the top grating is TiO_2 and the material of the sub grating is fused silica. The pitch of the 2D HCG is 453 nm. The line width of each grating is 220 nm. The height of both top and sub grating is 340 nm. The material of the substrate is the same as the sub grating.

TiO_2 was deposited on fused silica at HP Labs using a direct current magnetron sputter machine. The chamber pressure was 1.5 mTorr with an Ar flow about 100 sccm. The sputter power was 130 W and the rate was 4 nm/min. Two batches of TiO_2 film were sputtered at different temperatures, 27 °C and 270 °C respectively. To ensure an even film deposition, substrate stage rotation was turned on (20 rpm) during sputtering. Both batches of TiO_2 films were annealed at 300 °C for 3 hours after sputtering to improve film quality. After deposition, both batches of TiO_2 films were examined using a scanning electron microscope (SEM) (**Figure 4**). The refractive indices of TiO_2 films were also measured (**Figure 5**). The measured refractive indices were 10% lower than standard database, because the film was porous which can also be observed in **Figure 4**. A higher sputtering temperature could increase the refractive index, however the roughness of the film was much higher. To reach a good balance between refractive indices and film roughness, the TiO_2 film which was sputtered at 27 °C was chosen as the grating material.

The major steps for nanoimprint fabrication are schematically shown in **Figure 6**. First, a mold with certain patterns is pressed onto the UV-curable resist on the substrate. Then UV light is applied to cure the resist. After curing, the mold can be separated from the substrate and the shape of resist is exactly the opposite of the mold. The imprinted pattern can be used as the mask to etch the residual resist, deposit metal, lift off and finally etch into the substrate. In this way, the shape of the mold gets transferred into the substrate.

To fabricate 2D HCG, a mold is duplicated from a 1D periodic grating silicon master which was fabricated by interference lithography[12]. Then the same mold is used to imprint twice in orthogonal directions on the same silicon substrate to pattern a 2D hole array (**Figure 7**). The hybrid nanoimprint[13] process can make large-area samples with high-resolution and little defects. The imprinted results (2D hole array silicon array) is shown in **Figure 8**. The roughness of edges can be further reduced with the help of edge smoothing technologies[14].

After nanoimprint patterning and Cr mask array is completed, an ICP RIE machine is used to etch the sample. Two different etching recipes were developed for TiO_2 and fused silica respectively, which is shown in **Table 1**. The fabricated structure is shown in **Figure 9**.

The reflectance (from the normal incidence) of 2D HCG was measured using two different spectrometers with different types of detectors, the normal detector and the sphere integration detector. In contrast to sphere integration detector, the normal detector has a relatively small angle of acceptance and therefore will not receive the scattered light. As shown in **Figure 10**, the difference in reflectance curves measured by both detectors indicates that the light is scattered by the HCG due to the structure roughness. The difference between integration sphere measurement and simulation data is mainly due to the loss of material and fabrication errors. The reflectance curves can demonstrate that the fabricated device can work as a band reflector as one layer in the dispersive element. Due to the high contrast of index between the grating and the substrate, HCG has good angle independence. The reflectance curve will not change much when the incidence angle is less than 15°.

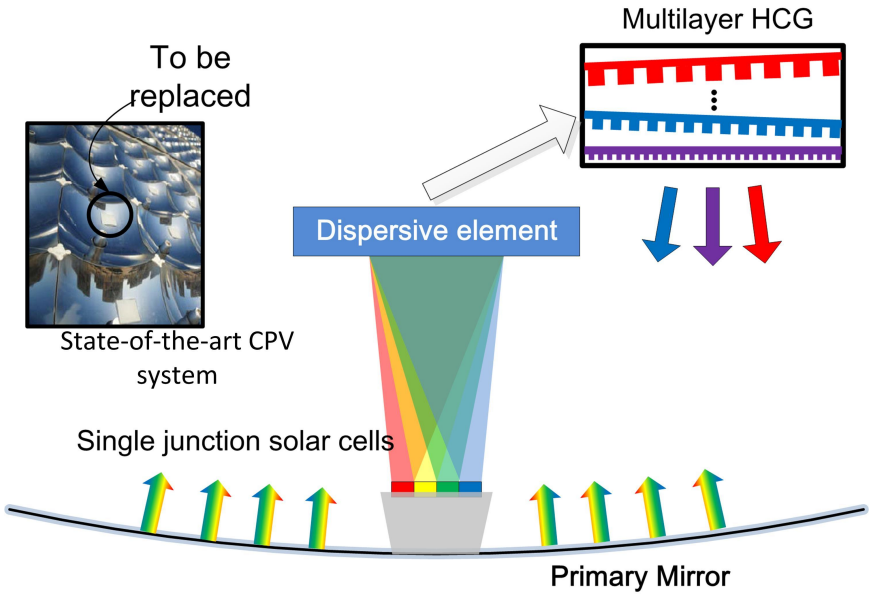

Figure 1. The implementation of the dispersive element (multiplayer HCG) in a concentrated photovoltaic (CPV) system.

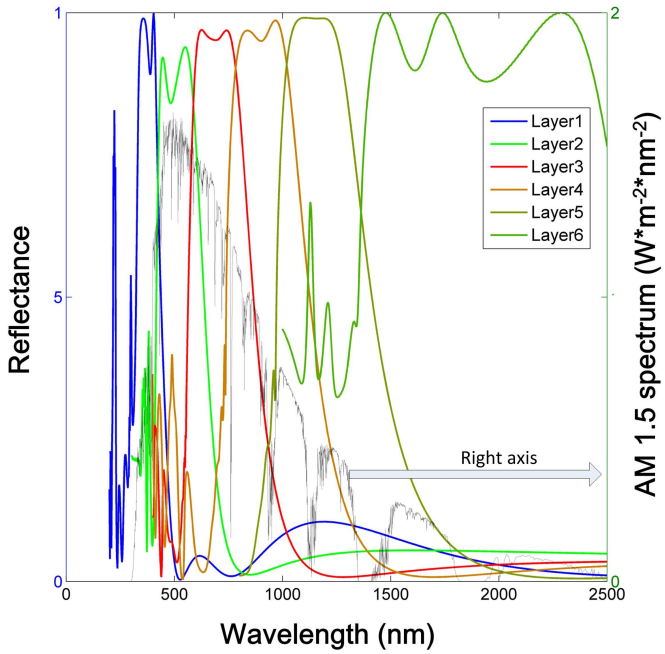

Figure 2. Numerically optimized reflectance curves for the dispersive element design (six-layer stacked HCG) that can cover most of the solar spectrum.

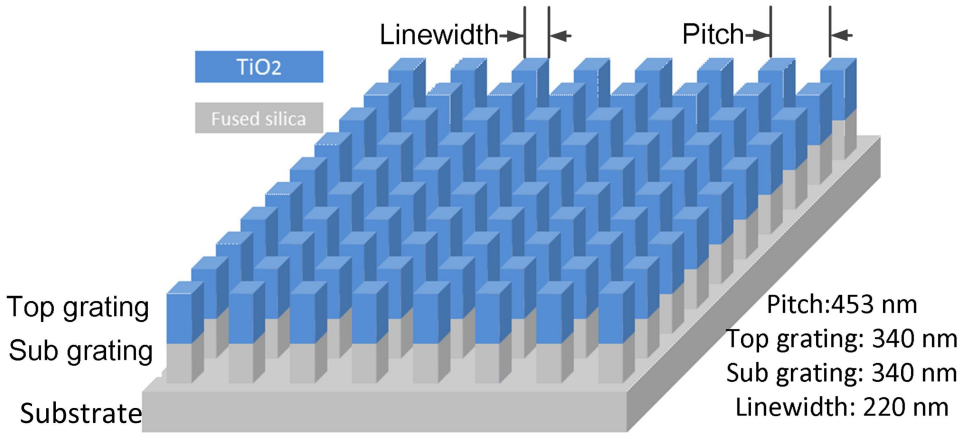

Figure 3. The optimized structure of a HCG for demonstration of nanoimprint fabrication.

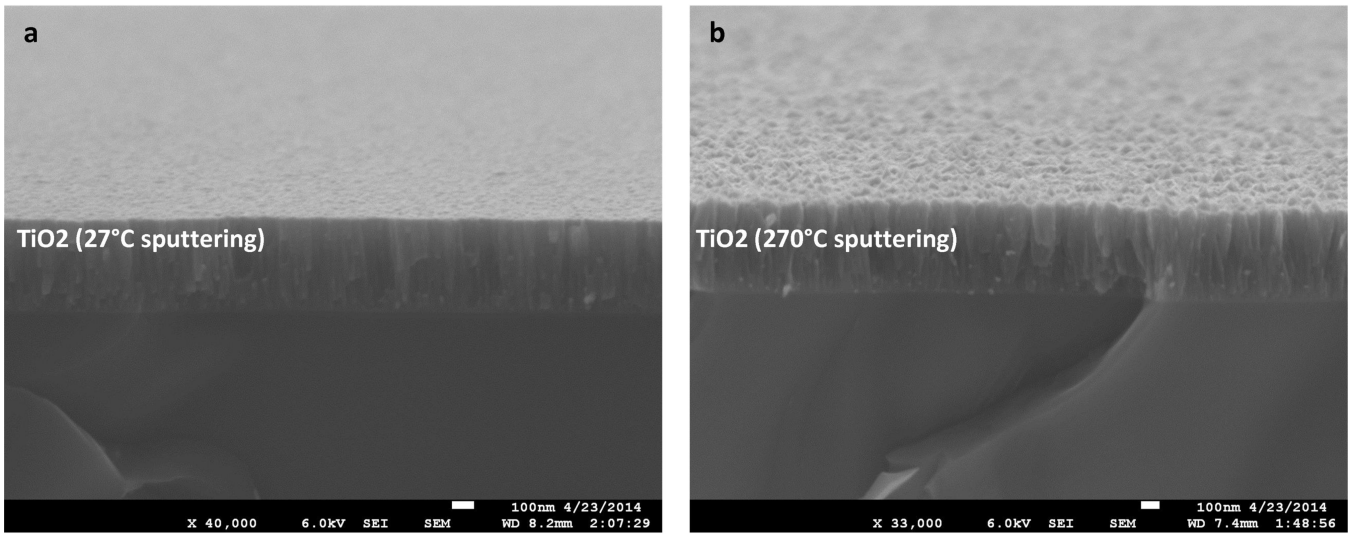

Figure 4. The SEM images (cross-sectional view) of sputtered TiO_2 films at (**a**) 27 °C and (**b**) 270 °C. Please click here to view a larger version of this figure.

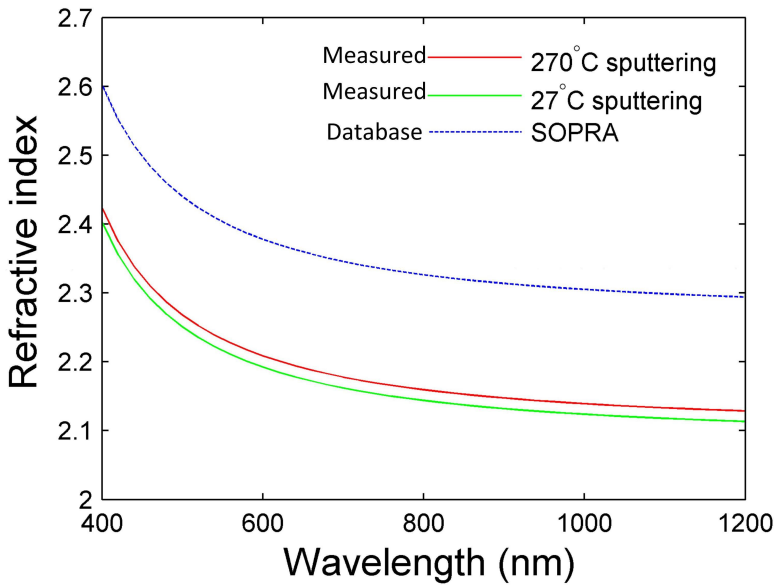

Figure 5. Measured and standard refractive (SOPRA database) indices of sputtered TiO_2 films.

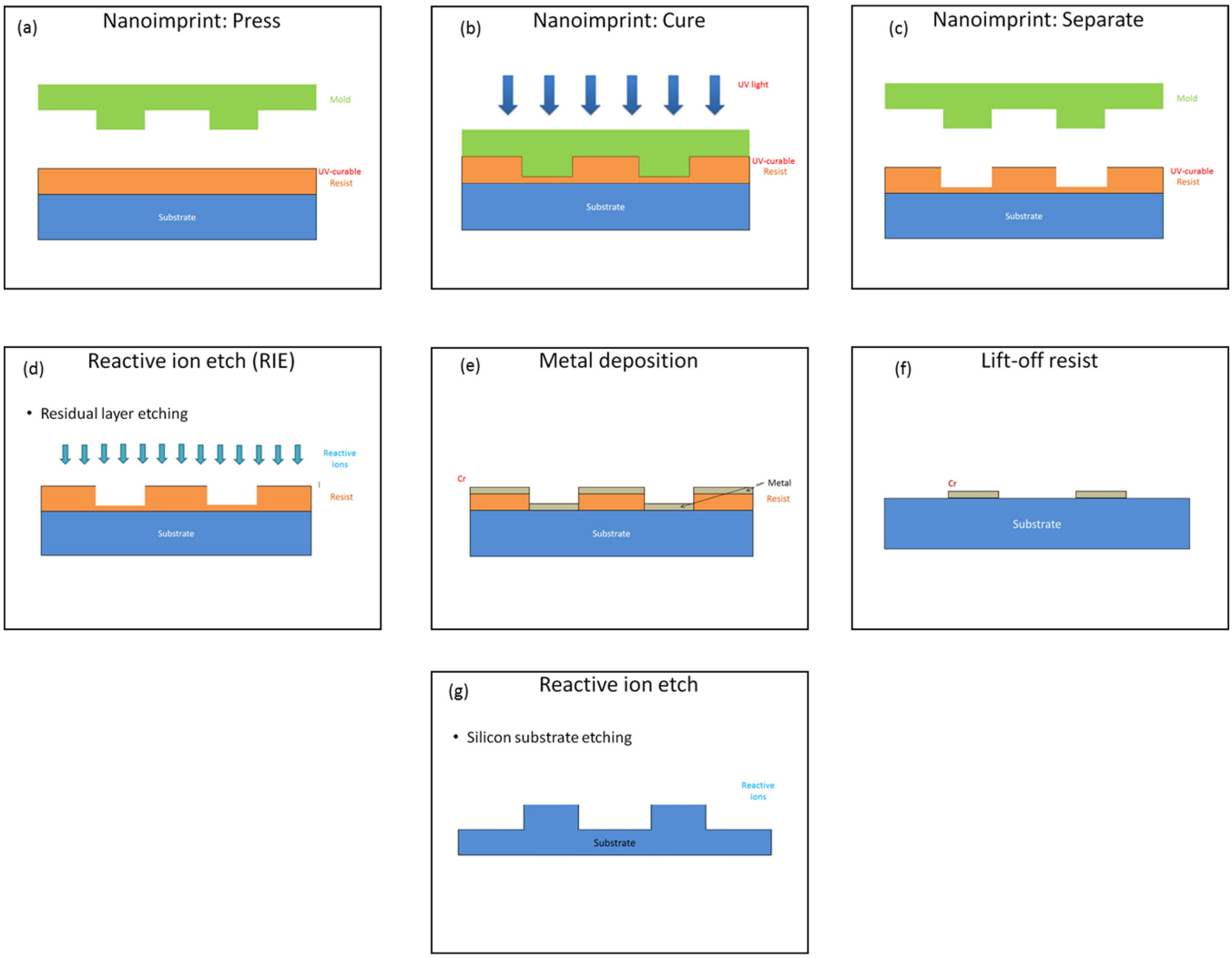

Figure 6. Nanoimprint fabrication process. Please click here to view a larger version of this figure.

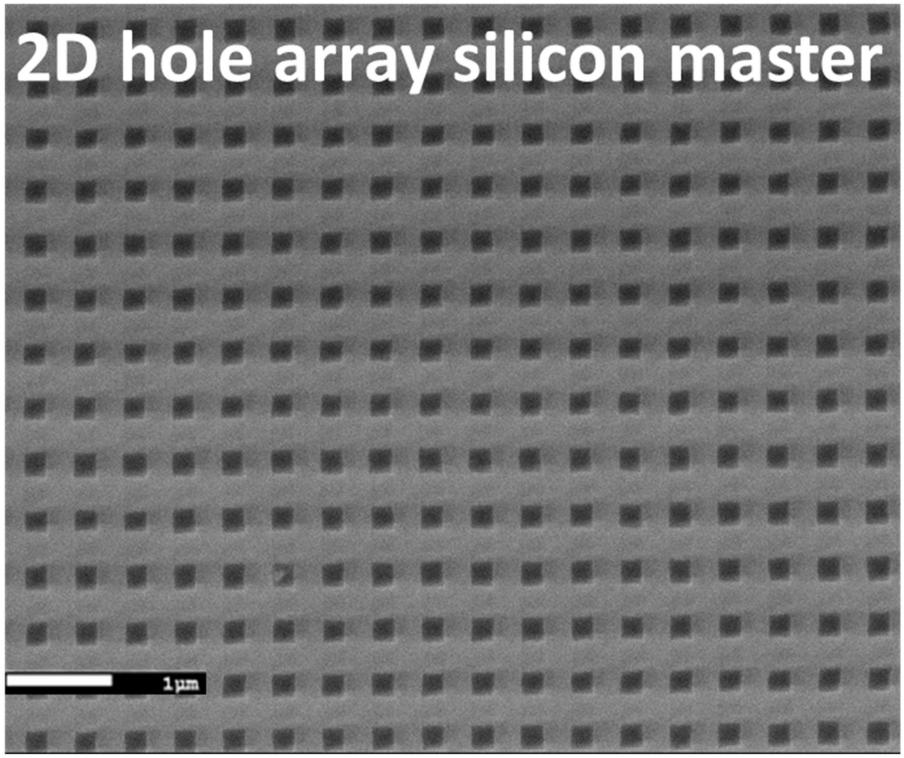

Figure 7. The SEM image of 2D hole array silicon master (top-down view).

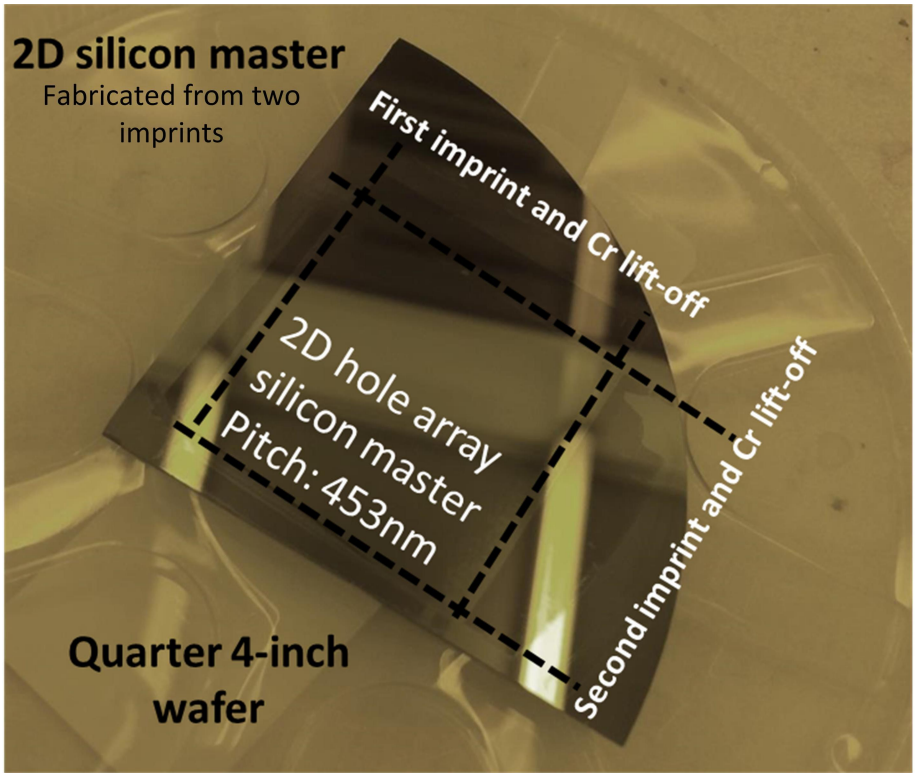

Figure 8. The photo of 2D hole array silicon master fabricated by PDMS-based nanoimprint.

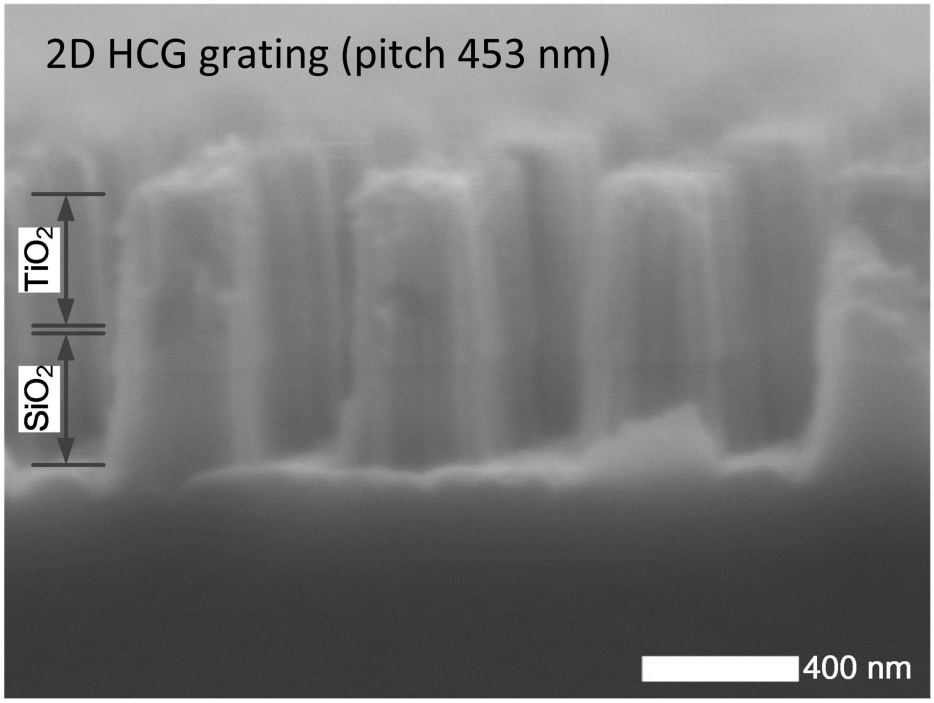

Figure 9. The SEM image (cross-sectional view) of the fabricated 2D HCG.

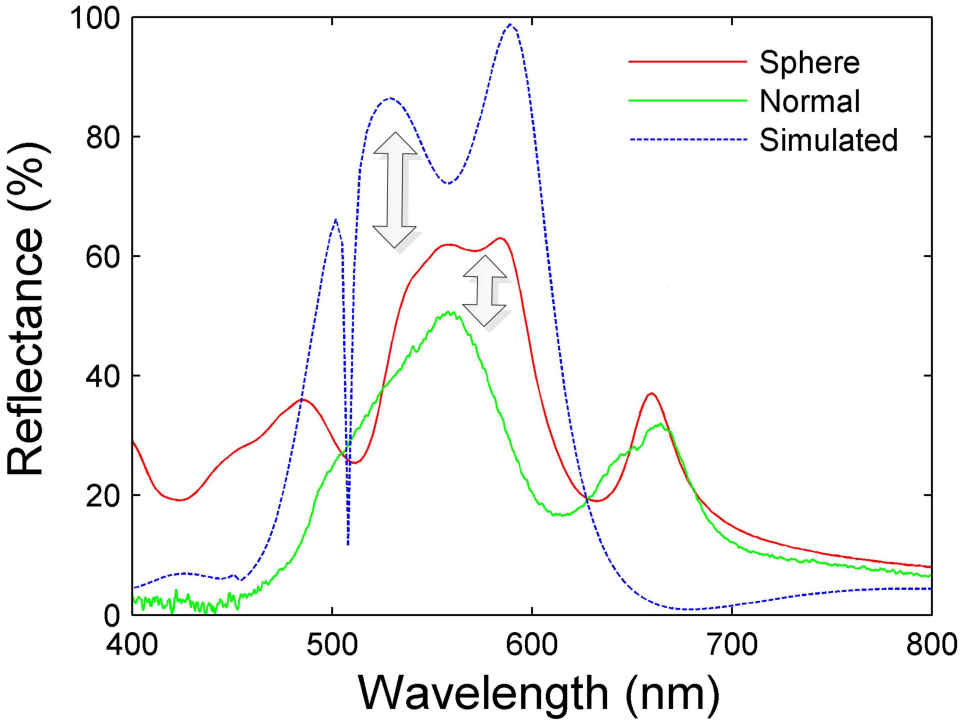

Figure 10. One simulated reflectance curve and two measured reflectance curves using sphere integration detector and normal detector respectively.

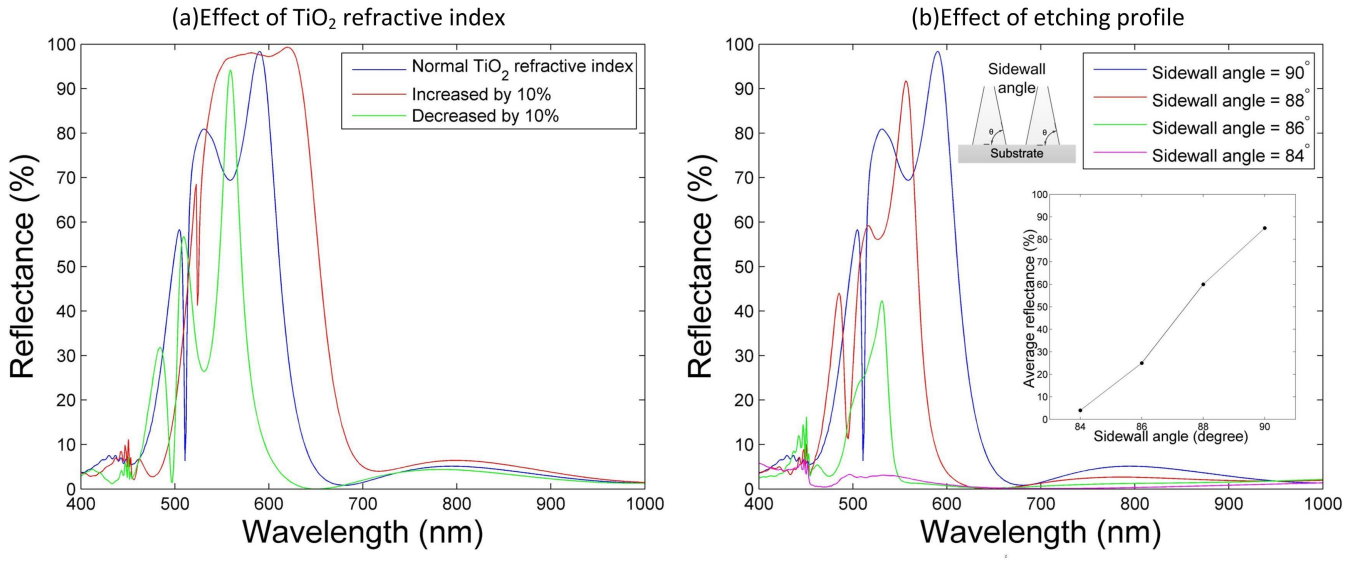

Figure 11. (**a**) Effect of refractive index on HCG reflectance; (**b**) Effect of sidewall angle on HCG reflectance. Please click here to view a larger version of this figure.

	ICP Power	Forward Power	SF_6 Flow	C_4F_8 Flow	O_2 Flow	Pressure	Etching Rate
TiO_2	0 W	25 W	25 sccm	10 sccm	10 sccm	10 mTorr	43 nm/min
Fused silica	0 W	100 W	0 sccm	15 sccm	15 sccm	10 mTorr	20 nm/min
Resist	0 W	25 W	25 sccm	15 sccm	0	10 mTorr	22 nm/min
PMMA	0 W	30 W	0	0	30 sccm	2 mTorr	55 nm/min
Clean	1,000 W	200 W	0	0	50 sccm	50 mTorr	NA

Table 1. The etching recipes for TiO_2, fused silica, UV resist, PMMA and clean.

Discussion

First, the quality of the TiO_2 film is very crucial for the HCG performance. The reflectance peak will be higher if the TiO_2 film has less loss and surface roughness. The TiO_2 film with a higher refractive index is also favorable because the optical mode confinement will be enhanced by a higher contrast in index, which can give rise to a flatter and broader reflectance band in HCG.

Second, the fabrication errors will have significant effects on the HCG and should be avoided. The roughness introduced in fabrication will cause more light to be scattered, so the reflectance will become lower. The deviation of parameters in HCG fabrication including line width, height and pitch will not allow the device to work optimally as in simulation. Moreover, the reflectance of HCG strongly depends on the etching profile, *i.e.* the angle of sidewall. In **Figure 11**, the effect of sidewall angles on the reflectance of HCG is numerically calculated. As the sidewall angles decrease from 90° to 84°, the average reflectance drops from over 90% to less than 50%, because the HCG behaves more like a cone-shaped anti-reflection coating when the sidewall angle is small.

The optical efficiency of the dispersive element is important for the overall efficiency of the CPV system, so the reflectance of each layer of HCG should be as high as possible. Based on the discussion above, while the optical efficiency for the fabricated layer is about 60%, there are several possible improvements for a better HCG reflectance. The TiO_2 sputtering condition can be further optimized to generate the film with a higher index, less surface roughness and lower optical loss. The dry etching recipes should be further adjusted for a better etching profile, making the grating straighter, which can be achieved by adjusting the combination of gases (C_4F_8, SF_6 and O_2) to balance the etching and re-deposition process. The nanoimprint and lift-off process should be improved to avoid roughness and fabrication errors so that the unnecessary scattering can be reduced to increase the overall optical efficiency.

By stacking multiple layers of two-dimensional HCGs with different pitches, the dispersive mirror can operate in much broader spectrum. The mirror can reflectively direct light into different angles according to wavelengths, in a way of packaging all HCG layers subsequently in different tilting angles. Moreover, the dispersive mirror can be fabricated using nanoimprint lithography (NIL) in a large area and at a low cost. Moreover, the proposed system features an easy integration with existing concentrator photovoltaic (CPV) setup so it has the potential to be accepted widely by the industry to improve solar energy conversion efficiency.

Disclosures

The authors have nothing to disclose.

Acknowledgements

This research was supported as part of the Center for Energy Nanoscience, an Energy Frontier Research Center funded by the U.S. Department of Energy, Office of Science under Award Number DE-SC0001013. We also want to thank Dr. Max Zhang and Dr. Jianhua Yang of HP Labs for their help on TiO_2 film sputtering and refractive indices measurement.

References

1. Horne, S. *et al.* A Solid 500 Sun Compound Concentrator PV Design. *Photovoltaic Energy Conversion, Conference Record of the 2006 IEEE 4th World Conference on.* 694-697, doi: 10.1109/WCPEC.2006.279550 (2006) .
2. Guter, W. *et al.* Current-matched triple-junction solar cell reaching 41.1% conversion efficiency under concentrated sunlight. *Applied Physics Letters.* **94**, 223504 , doi: 10.1063/1.3148341 (2009).
3. Shockley, W., & Queisser, H. J. Detailed Balance Limit of Efficiency of p-n Junction Solar Cells. *Journal of Applied Physics.* **32**, 510-519, doi: 10.1063/1.1736034 (1961).
4. Green, M. A. Potential for low dimensional structures in photovoltaics. *Materials Science and Engineering: B.* **74**, 118-124, doi: 10.1016/S0921-5107(99)00546-2 (2000).
5. Karagodsky, V., & Chang-Hasnain, C. J. Physics of near-wavelength high contrast gratings. *Opt. Express.* **20**, 10888-10895, doi: 10.1364/OE.20.010888 (2012).
6. Chou, S. Y., Krauss, P. R., & Renstrom, P. J. Nanoimprint lithography. *Journal of Vacuum Science & Technology B: Microelectronics and Nanometer Structures.* **14**, 4129-4133, doi: 10.1116/1.588605 (1996).
7. Namiki, T. A new FDTD algorithm based on alternating-direction implicit method. *Microwave Theory and Techniques, IEEE Transactions on.* **47**, 2003-2007, doi: 10.1109/22.795075 (1999).
8. Moharam, M. G., & Gaylord, T. K. Rigorous coupled-wave analysis of planar-grating diffraction. *J. Opt. Soc. Am.* **71**, 811-818, doi: 10.1364/josa.71.000811 (1981).
9. Smilab, S. nk Database. *World Wide Web.* http://www.sopra-sa.com (2015).
10. Yao, Y., Liu, H., & Wu, W. Spectrum splitting using multi-layer dielectric meta-surfaces for efficient solar energy harvesting. *Appl. Phys. A.* **115**, 713-719, doi: 10.1007/s00339-014-8419-y (2014).
11. Yao, Y., Liu, H., & Wu, W. Fabrication of high-contrast gratings for a parallel spectrum splitting dispersive element in a concentrated photovoltaic system. *Journal of Vacuum Science & Technology B.* **32**, 06FG04-06FG04-6, doi: 10.1116/1.4898198 (2014).
12. Solak, H. H. *et al.* Sub-50 nm period patterns with EUV interference lithography. *Microelectronic Engineering.* **67**, 56-62, doi: 10.1016/S0167-9317(03)00059-5 (2003).
13. Li, Z. *et al.* Hybrid nanoimprint− soft lithography with sub-15 nm resolution. *Nano letters.* **9**, 2306-2310, doi: 10.1021/nl9004892 (2009).
14. Yu, Z., Chen, L., Wu, W., Ge, H., & Chou, S. Y. Fabrication of nanoscale gratings with reduced line edge roughness using nanoimprint lithography. *Journal of Vacuum Science & Technology B.* **21**, 2089-2092, doi: 10.1116/1.1609471 (2003).

